First-principles study of Fe/MgO based magnetic tunnel junctions with Mg interlayers

Yan Wang,[1,2] Jia Zhang,[1] X.-G. Zhang,[3] Hai-Ping Cheng,[2] and X. F. Han[1]
[1]*Beijing National Laboratory for Condensed Matter Physics, Institute of Physics, Chinese Academy of Sciences, Beijing 100190, China*
[2]*Department of Physics and Quantum Theory Project, University of Florida, Gainesville, Florida 32611, USA*
[3]*Center for Nanophase Materials Sciences and Computer Science and Mathematics Division, Oak Ridge National Laboratory, Oak Ridge, Tennessee 37831-6164, USA*

(Received 19 March 2010; revised manuscript received 13 July 2010; published 4 August 2010)

-Fe(001)/Mg/MgO/Fe- and -Fe(001)/Mg/MgO/Mg/Fe- magnetic tunnel junctions (MTJs) with Mg interlayers are studied by first-principles calculations. We find that the Mg interlayer is able to preserve the preferential transmission of the majority-spin states with Δ_1 symmetry, which dominates the spin-dependent electron transport in MTJs with MgO barrier. A monoatomic layer of Mg at the electrode/barrier interface does not decrease the tunneling magnetoresistance (TMR) ratio nearly as much as a similar layer of iron oxide. We also find that at a certain Mg thickness the TMR is strongly influenced by resonant tunneling in the minority-spin channel. These resonances are due to the coupling between the quantum-well states within the Mg interlayer to the interfacial resonance states on the Fe/Mg interface. The calculated results are used to explain experimental measurements of MTJs with Mg interlayers.

DOI: 10.1103/PhysRevB.82.054405 PACS number(s): 72.25.Mk, 73.40.Gk, 73.40.Rw

I. INTRODUCTION

Since the theoretical prediction[1,2] and the subsequent experimental observation[3,4] of giant tunneling magnetoresistance (TMR) effect in magnetic tunnel junctions (MTJs) with single-crystalline MgO(001) barrier, such MTJs have found wide applications in spin-electronics devices including read heads in hard disk drives, magnetic random access memories, and magnetic sensors and logics. Extensive studies have been made to improve the junction quality as well as the TMR ratio, i.e., by optimizing the material, structure, and the growth condition of the MTJs.[5–8] These efforts have led to recent records of room-temperature TMR of 604% for single-barrier MTJs (Ref. 9) and 1056% for double-barrier MTJs.[10]

One of the experimental techniques already widely adopted for making high-quality MgO-based MTJs is to deposit an ultrathin Mg layer on top of the bottom ferromagnetic electrode layer prior to the deposition of MgO[11–17] or to insert a Mg interlayer at each electrode/barrier interface of the junction.[18] The advantages of inserting Mg interlayers include (1) the slightly but not fully oxidized Mg layer yields a low-resistance-area product of the junction while maintaining a high TMR ratio at the same time.[11] (2) It can also serve as a crystalline seed so that the texture of the subsequently deposited MgO(001) barrier as well as the junction interface can be much improved.[11,12,16,17] (3) Possible oxidation of the electrode at the junction interface can be avoided,[13–16] which, in turn, improves the TMR ratio since the formation of FeO on the interface greatly reduces the TMR.[19–24] There is experimental evidence that the spin symmetry of the bulk Fe Bloch states may be maintained well into a Mg interlayer as thick as 10 Å.[12] The measured TMR strongly depends on the Mg thickness, and the maximum usually occurs at the nominal Mg thickness of 2–4 Å.[12,13,16]

The reason for the very high TMR in the MgO-based MTJs is understood to be the spin symmetry filtering effect of the MgO(001) barrier which preferentially transmits the majority-spin Δ_1 electrons.[1] How the insertion of a Mg interlayer on the Fe/MgO interface affects the spin symmetry filtering effect cannot be studied by experiments alone. Previously, first-principles calculations have been applied to study the role of interface oxide layer,[19–24] amorphous Fe interlayer,[25,26] as well as other interlayers of Co,[27,28] V,[29] Cr,[28] and Ag.[30] Similarly, here first-principles calculation is also a critical step in understanding the role of Mg interlayer in these experiments.

In this paper, we report a first-principles study of the electronic structure and transport properties of both asymmetric -Fe(001)/Mg/MgO/Fe- and symmetric -Fe(001)/Mg/MgO/Mg/Fe- MTJs. We assume a body-centered tetragonal crystalline structure of Mg which can be matched epitaxially with the Fe(001) electrode as well as the MgO(001) barrier. We show that except for the majority-spin states with Δ_1 symmetry, all other bulk Bloch states from the Fe electrode decay exponentially in the Mg interlayer. Thus, the Mg interlayer does not simply prevent the interface oxidation or improves the texture of subsequently deposited MgO(001). It also preserves the preferential transmission of the majority-spin Δ_1 electrons which is the reason for high TMR ratio in MgO-based MTJs. For Mg interlayer with thickness of 2 ML the TMR is strongly influenced by resonant tunneling due to the quantum-well states (QWS) within the Mg interlayers. These *sp*-like QWS are effectively coupled to the interfacial resonant states (IRS) on the Fe/Mg interface and have a large contribution to the minority-spin transport. The calculation results are used to explain quite a number of recent experiments using Mg as interlayer.[11–18]

The rest of the paper is organized as follows. In Sec. II we describe the detailed junction structures, interfaces, and the computational methodology for both interface-structure relaxation and tunneling transport calculations. In Sec. III we report the spin-dependent transport properties with the main focus on the majority-spin transport in the Mg interlayer. In Sec. IV the Mg thickness dependence of the junction resistance and the TMR are presented and are compared with experiments. The resonant tunneling effect in minority-spin

channel due to coupling of interfacial resonance states and quantum-well states are discussed in Sec. V. In Sec. VI we present the conclusion.

II. INTERFACE STRUCTURES AND COMPUTATIONAL APPROACH

In the asymmetric -Fe/Mg/MgO/Fe- junction there are two different interfaces. For the top interface of Fe/MgO, we use the same structure as in Ref. 1. For the bottom Fe/Mg/MgO interface we assume that the Mg interlayer with a few (0–5) ML thickness has the same bcc structure (with a tetragonal distortion, see below) of the Fe(001) electrode and that the Mg sites are on top of the O atoms at the Mg/MgO interface. Thicker interlayer of Mg may introduce large lattice disorder in experiments which will not be discussed in this paper. The (001) in-plane Mg lattice is fixed at the bulk Fe (electrodes) lattice constant of 2.866 Å, and the MgO lattice constant in the same plane is taken to be a factor of $\sqrt{2}$ larger than that of the Fe. Thus all layers in the junction are matched epitaxially. The out-of-plane MgO lattice (along the [001] axis) is set as 2.21 Å which is taken from experiment.[4]

Plane-wave pseudopotential code of the QUANTUM-ESPRESSO distribution[31] is used to optimize the interlayer distances of Fe-Mg, Mg-Mg, and Mg-MgO. The Fe(001)/Mg/MgO interface structure is modeled by a 21-atom supercell with six (001) Fe layers, three (001) Mg layer, and six (001) MgO layers. The in-plane lattice constant is fixed while all atomic coordinates are allowed to relax in the direction perpendicular to the layers. Perdew-Wang (PW-91) (Ref. 32) generalized gradient approximation exchange-correlation density functionals are used with an energy cutoff of 700 eV and a $9\times9\times1$ Monkhorst-Pack grid,[33] and Vanderbilt ultrasoft pseudopotentials[34] have been employed. Optimization proceeds until the [001]-axis component of the force on each atom is lower than 0.05 eV/Å. Relaxation calculation yields a layer spacing of 1.837 Å for Fe-Mg distance and 2.943 Å for Mg-MgO distance. The Mg-Mg spacing is taken to be the average of two Mg-Mg spacings (2.589 and 2.550 Å) which yields 2.570 Å and is set to be independent of the Mg interlayer thickness in subsequent transport calculations.

The electronic structure and transport calculations for the junction are carried out using the layer Korringa-Kohn-Rostoker (Layer-KKR) implementation[35] of density-functional theory and local spin-density approximation, where the junction is divided into three parts: two semi-infinite bcc Fe(001) electrodes and a center region as illustrated in Fig. 1 produced by the XCRYSDEN (Ref. 36) graphical package. The application of the Layer-KKR method to MgO-based MTJs is in a similar manner as in the past works.[1,19,37,27]

For the atomic sphere approximation, the size of the Fe atomic spheres is the same as in Refs. 1, 27, and 37. The spheres for Mg and O are enlarged proportionally in order to correctly account for the volume of each layer due to the increased out-of-plane lattice spacing of MgO. An empty sphere of radii 1.668 Å(0.875 Å) is inserted in the interfacial Mg (Fe) layer just beside the Mg atom of adjacent MgO layer displaced 0.067 Å toward the MgO. Additional empty

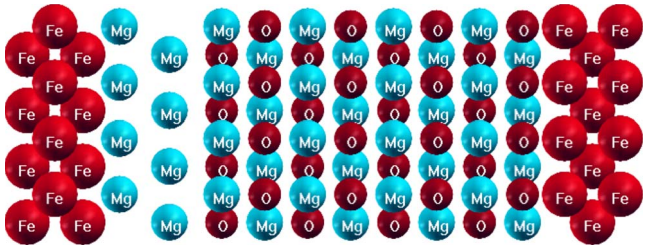

FIG. 1. (Color online) Atomic structure of the center region in the -Fe/Mg/MgO/Fe- system with eight atomic layers of MgO(001) barrier and two atomic layers of Mg(001) interlayer.

spheres of radii 1.570 Å are placed in other Mg layers when the Mg interlayer thickness is larger than 1 ML. The angular-momentum cutoff is $l=3$. The self-consistent calculation is performed in the same manner as in Refs. 1, 27, and 37. Once the electronic structure is converged, the tunneling conductance is calculated using the Landauer-Büttiker conductance formalism implemented within the first-principles Layer-KKR framework.[35] The imaginary part of the energy for the transport calculation is 2.7×10^{-6} eV.

III. SPIN-DEPENDENT TRANSPORT

The calculated transmission probability of -Fe/Mg/MgO/Fe- as a function of $\mathbf{k}_{\parallel}(k_x,k_y)$ with 1024×1024 $\mathbf{k}_{\parallel}$ points in the two-dimensional Brillouin zone (2DBZ) is shown in Fig. 2 for different spin channels. The majority-spin to majority-spin conductance is dominated by a broad peak centered at $\mathbf{k}_{\parallel}=0$, similar to the cases of -Fe/MgO/Fe- and -Fe/Co/MgO/Co/Fe- MTJs.[1,27] Majority Δ_1 states are identified to be the primary source of the peak and tunneling Δ_1 states far away from the center of the 2DBZ decay faster than those close to the center.[1,38] In the other configurations, the conductances are characterized by sharp peaks close to the center of the 2DBZ, especially for the minority-spin channel in the antiparallel (AP) configuration. Similar so-called *hot spots* have been associated with resonant tunneling due to IRS in various junctions.[1,27,39] The resonant tunneling hot spots are off

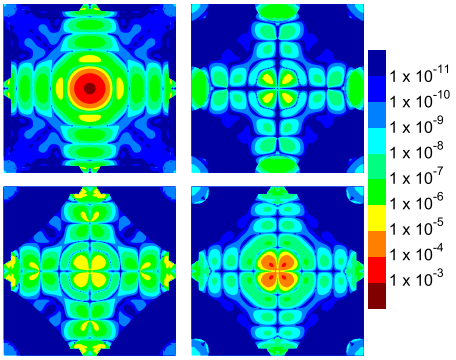

FIG. 2. (Color online) Transmission probability as a function of $\mathbf{k}_{\parallel}$ in 2DBZ for -Fe/Mg(1 ML)/MgO/Fe- at the Fermi energy. The four panels show the transmission for majority-spin (upper left) and minority-spin (upper right) in the parallel configuration, as well as majority-spin to minority-spin (lower left) and minority-spin to majority-spin (lower right) in the antiparallel configuration.

TABLE I. Tunneling conductivity (unit: $1/\Omega m^2$) in various spin channels and conductance ratio of G_P/G_{AP} for -Fe/MgO/Fe-, -Fe/Mg(1 ML)/MgO/Fe-, and -Fe/FeO(1 ML)/MgO/Fe- tunnel junctions. MgO barrier thickness is set to 8 ML for all cases.

Structure	$G_P^{\uparrow\uparrow}$	$G_P^{\downarrow\downarrow}$	$G_{AP}^{\uparrow\downarrow}$	$G_{AP}^{\downarrow\uparrow}$	TMR ratio (%)
-Fe/MgO/Fe-	7.85×10^9	1.19×10^9	5.91×10^7	5.91×10^7	7548
-Fe/Mg/MgO/Fe-	6.61×10^9	2.07×10^7	9.21×10^7	5.86×10^8	878
-Fe/FeO/MgO/Fe-	2.90×10^8	2.70×10^7	1.02×10^7	1.36×10^8	117

the axes $k_x=0$ and $k_y=0$ in the 2DBZ. This is because the Bloch states along these lines do not have s character and they can only couple to evanescent states in the MgO layer that decay rapidly. On the other hand, the states slightly away from the axes can couple to the evanescent states in the MgO layer that decay more slowly.

Summing the transmission probability over the entire 2DBZ with 1024×1024 $\mathbf{k}_\parallel$ points in Fig. 2, we find the tunneling conductivity of -Fe/Mg/MgO/Fe- for each spin channel, as is shown in Table I. $G_P^{\uparrow\uparrow}$, $G_P^{\downarrow\downarrow}$, $G_{AP}^{\uparrow\downarrow}$, and $G_{AP}^{\downarrow\uparrow}$ are the majority and minority spin channels for parallel (P) configuration, majority-to-minority and minority-to-majority spin channels for antiparallel configuration, respectively. The junction conductivities of the parallel and antiparallel configurations are summed from two spin-dependent channels as $G_P=G_P^{\uparrow\uparrow}+G_P^{\downarrow\downarrow}$ and $G_{AP}=G_{AP}^{\uparrow\downarrow}+G_{AP}^{\downarrow\uparrow}$. The TMR ratio is defined as

$$\mathrm{TMR}=\frac{R_{AP}-R_P}{R_P}=\frac{G_P-G_{AP}}{G_{AP}}\times100\%,\quad R_{AP}>R_P, \quad (1)$$

$$\mathrm{TMR}=\frac{R_{AP}-R_P}{R_{AP}}=\frac{G_P-G_{AP}}{G_P}\times100\%,\quad R_{AP}<R_P, \quad (2)$$

where the R_{AP} and R_P are the junction resistance for P and AP configurations, respectively. For some cases due to the dominant contribution from resonant tunneling to the AP conductance, the TMR becomes negative. These results will be discussed in Sec. IV. The results of junctions -Fe/MgO/Fe- with perfect interface and -Fe/FeO/MgO/Fe- with 1 ML interface oxidation FeO layer are also presented in Table I for comparison. The FeO/MgO interface structure of -Fe/FeO/MgO/Fe- is the same as a previous study[19] of the interface oxidation for -Fe/MgO/Fe-.

As shown in Table I, in majority-spin channel the conductivity $G_P^{\uparrow\uparrow}$ of -Fe/Mg/MgO/Fe- is very close to the results for -Fe/MgO/Fe- but much larger than the -Fe/FeO/MgO/Fe-. Not surprisingly, we get a relatively large conductivity for the AP configuration of -Fe/Mg/MgO/Fe-, especially the $G_{AP}^{\downarrow\uparrow}$ due to a large contribution from resonant tunneling which dominates the AP minority-spin channel. The calculated conductance ratio for -Fe/Mg/MgO/Fe- is smaller than that of

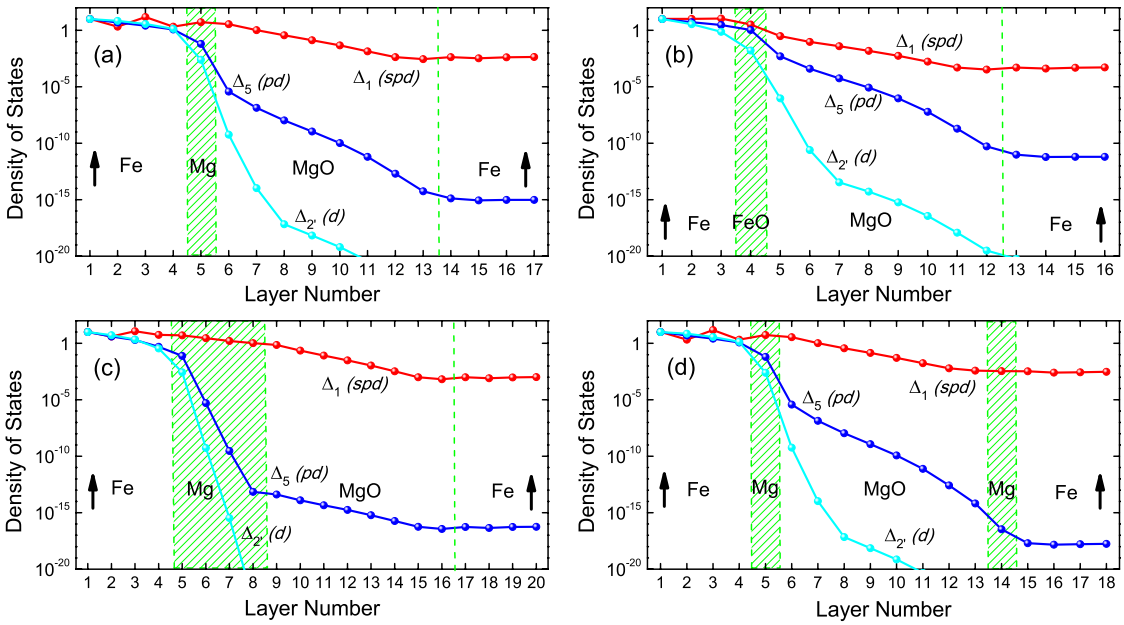

FIG. 3. (Color online) TDOS on each atomic layer of (a) -Fe/Mg(1 ML)/MgO/Fe-, (b) -Fe/FeO(1 ML)/MgO/Fe-, (c) -Fe/Mg(4 ML)/MgO/Fe-, and (d) -Fe/Mg(1 ML)/MgO/Mg(1 ML)/Fe- for $\mathbf{k}_\parallel=0$ with parallel configuration. Each TDOS curve is labeled by the symmetry of the incident Bloch state in the left Fe electrode at the Fermi energy. Shadow area and dashed line represent the Mg interlayer and the Fe/MgO interface, respectively. Arrows represent the relative magnetization in the Fe electrodes.

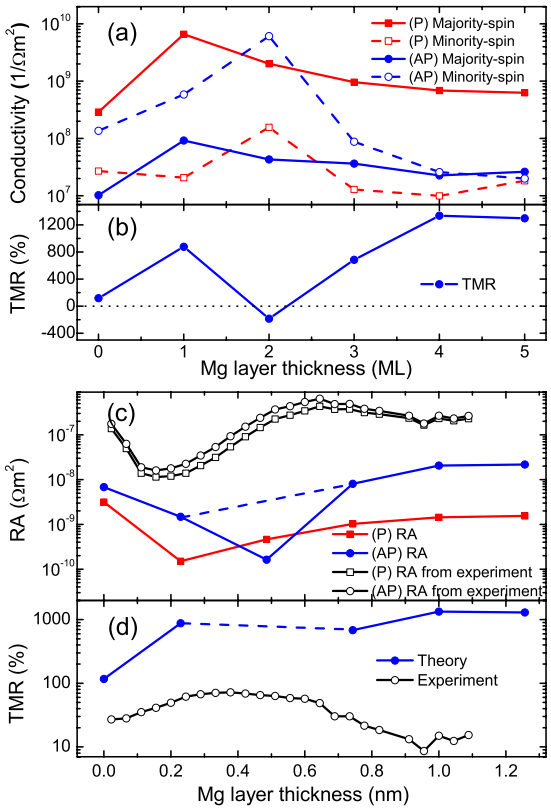

FIG. 4. (Color online) (a) Mg-layer thickness dependence of tunneling conductivity in various spin channels, (b) TMR ratio in linear scale and (d) log scale, and (c) resistance-area product for the -Fe/Mg/MgO/Fe- tunnel junctions with MgO thickness of 1.77 nm, in comparison with the cited experimental results for -FeCo/Mg/MgO/FeCo- junctions with MgO thickness of 1.98 nm (Ref. 13). The interfacial FeO with 1 ML is assumed for the case with 0 ML of Mg. The dashed lines connecting the data points of 1 and 3 ML in (c) and (d) indicate the trends without the 2 ML resonant tunneling anomaly.

-Fe/MgO/Fe-. The main reason for the reduction is the large difference in the $G_{\mathrm{AP}}^{\downarrow\uparrow}$ channel. Nevertheless, the calculated TMR ratio with a Mg interlayer is much higher than that of -Fe/FeO/MgO/Fe- with an FeO interlayer. This result explains why the insertion of a Mg interlayer or underoxidization of MgO in experiments can improve TMR: an extra layer of Mg largely preserves the dominant tunneling current in the majority-spin channel and prevents the formation of an interface FeO layer which would reduce the TMR much more than the Mg interlayer. The observed boost of TMR in experiment is resulting from the replacement of interfacial oxidation layer by the Mg interlayer.

Next we examine the tunneling density of states (TDOS) at $\mathbf{k}_{\parallel}=0$ for the individual energy bands in the majority-spin channel. The TDOS is defined as the electron density of states at each layer due to a single incident Bloch state from the left Fe electrode. On each atomic layer, the TDOS is roughly proportional to the modular square of the wave function that matches to the incident Bloch state. The plots for the TDOS in Fig. 3 illustrate the most important feature of this paper. For bcc Fe(001) in the majority channel there are four Bloch states at the Fermi energy for $\mathbf{k}_{\parallel}=0$ with different symmetries: a Δ_1 state, a doubly degenerate Δ_5 state, and a $\Delta_{2'}$ state. As shown clearly in Fig. 3(a), the majority-spin state with Δ_1 symmetry can pass through the Mg layer effectively while Δ_5 and $\Delta_{2'}$ states cannot. The TDOS of Δ_1 states in the Mg interlayer show consistent transmitting from left Fe layers into the adjacent MgO layer without any sign of decay, but for other states the TDOS show remarkably large decay in the Mg layer. After passing through this Mg layer, the Δ_1 state starts to decay exponentially in the barrier MgO layers, as the same as other tunneling states.

For the junction with 1 ML FeO interface layer in Fig. 3(b), the Δ_1 state decays rapidly in the FeO layer, consistent with the large $G_{\mathrm{P}}^{\uparrow\uparrow}$ difference between -Fe/Mg/MgO/Fe- and Fe/FeO/MgO/Fe- shown in Table I. The difference between the TDOS in -Fe/Mg/MgO/Fe- and that in -Fe/FeO/MgO/Fe- connects the larger TMR in the case with a Mg interlayer with the different decay rates of the majority-spin Δ_1 state for the two cases. The slower decay of the Δ_1 electrons in the Mg interlayer is further confirmed when the Mg interlayer thickness is increased to 4 ML or when an additional Mg interlayer is inserted into the other interface in a symmetric -Fe/Mg/MgO/Mg/Fe- junction, as shown in Figs. 3(c) and 3(d). In Fig. 3(c), it is clear that the decay rate of Δ_1 state in Mg is much smaller than in the MgO barrier, but the TDOS for other symmetry states decreases rapidly with a decay rate much larger than within the MgO barrier. It is also worth noting that modification of the interface distances of Fe-Mg and Mg-MgO will only slightly change the calculated conductivity but does not have an impact on the qualitative behavior of the majority-spin Δ_1 electron transport in the Mg interlayer.

IV. MG INTERLAYER THICKNESS DEPENDENCE OF TMR AND COMPARISON WITH EXPERIMENTS

The dependence of spin-dependent transport on the Mg interlayer thickness is one aspect of the calculation that can be directly compared to the experiments. The tunneling conductance of -Fe/Mg/MgO/Fe- for each channels, $G_{\mathrm{P}}^{\uparrow\uparrow}$, $G_{\mathrm{P}}^{\downarrow\downarrow}$, $G_{\mathrm{AP}}^{\uparrow\downarrow}$, and $G_{\mathrm{AP}}^{\downarrow\uparrow}$, as well as the TMR ratio are shown in Fig. 4 with different interlayer Mg thickness up to 5 ML. To directly compare to the experiments we assume that for the junction without a Mg interlayer (0 ML case), an 1-ML-thick FeO interlayer is present at the interface. The results are plotted in Fig. 4. In the presence of a Mg interlayer, in Fig. 4(a) we only find small changes for majority-spin conductances in both P and AP configurations as the thickness of Mg varies. However, the minority-spin conductances in both configurations have large variations with different Mg thicknesses, and the changes in the conductance with the increasing Mg thickness are not mononomic. We also see an abrupt increase in conductance for minority-spin channel in each configuration at 2 ML Mg thickness. This abrupt increase in the conductance is due to resonant tunneling and will be discussed in the next section.

We now compare our calculated Mg thickness dependence of resistance-area (RA) product and TMR with the experimental measurements by Moriyama *et al.*[13] for -FeCo/Mg/MgO/FeCo- junctions with MgO thickness of 1.98 nm,

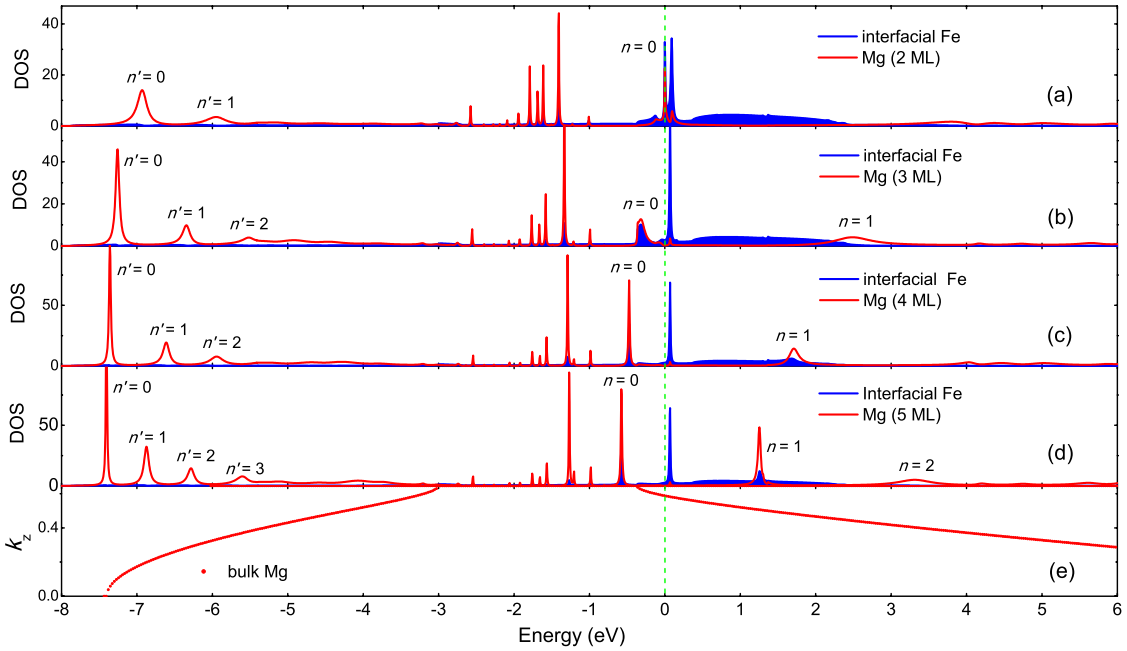

FIG. 5. (Color online) (a)–(d) Minority-spin density of states in Mg and interfacial Fe layers at the $\mathbf{k}_\parallel$ equal to one of the resonance peaks in transmission (junction with 2 ML Mg) for Mg interlayer thickness of 2, 3, 4, and 5 ML, respectively. Red (light) line, Mg layer; blue (dark) line (area filled under curve), adjacent Fe interfacial layer. (e) Band dispersion of bulk Mg using the same crystal structure in the junction. Dashed line represents the Fermi energy which is at 0 eV. n and n' indicate the numbers of nodes in the wave function corresponding to the two bulk Mg bands, respectively.

as shown in Figs. 4(c) and 4(d). The experimental values of RA are higher due to the difference between the experimental MgO thickness (1.98 nm) and the MgO thickness of 1.77 nm used in our calculation. If we exclude the case of 2 ML Mg in the AP configuration which contains a large resonant tunneling contribution and will be discussed in the next section, the calculated thickness dependences of RA in both configurations as well as the TMR follow almost the same trend as the experiment in the small thickness region (0.6 nm), as shown in Figs. 4(c) and 4(d). The dashed lines in both theory curves connecting the data points of 1 and 3 ML of Mg represent the trend if the 2 ML anomaly is removed. In the large thickness region the experimental TMR ratio is decreasing whereas the calculated TMR is further increasing. The discrepancy may coming from the degraded (001) texture of the MgO barrier when the Mg thickness is larger than 0.6 nm.[12,16]

V. RESONANT TUNNELING THROUGH INTERFACIAL RESONANT STATES AND QUANTUM-WELL STATES

At 2 ML layer Mg thickness, *sp*-like QWS are formed in the Mg interlayer. In Fig. 5(a), we show the calculated minority-spin DOS within the Mg interlayers and the adjacent Fe interfacial layer in -Fe/Mg/MgO/Fe- junction, at the one of the resonance peaks in the $\mathbf{k}_\parallel$-resolved transmission probabilities shown in Fig. 6 for the junction with 2 ML Mg. DOS at the same $\mathbf{k}_\parallel$ point for Mg thicknesses of 3, 4, and 5 ML, as well as the band dispersion $E(k_z)$ of bulk Mg using a crystal structure of body-centered tetragonal as the same in the junction, are also shown in Figs. 5(b)–5(e) for comparison. For each case the DOS of Mg are summed over all Mg layers between Fe and MgO. Band dispersion of bulk Mg is calculated using the Layer-KKR with the potentials for Mg taken from the center Mg layer of the -Fe/Mg/MgO/Fe- junction in order to correctly place the Fermi energy. Two bulk bands start at about 0.5 eV and 7.5 eV below the Fermi energy, respectively. Within the energy range corresponding to these two bulk bands, several sharp spikes in the junction partial DOS of Mg (primarily *s* and *p* characters) indicate possible QWS derived from the two bulk Mg bands, shown in Figs. 5(a)–5(d) for each Mg thickness.

That these sharp peaks are indeed the QWS is confirmed with the simple phase accumulation model (PAM, also referred to as the Bohr-Sommerfeld quantization rule) for the quantization condition of QWS.[37,40,41] According to the PAM, the quantization condition for the existence of a QWS with energy E_{QW} is given by

$$2k_\perp d + \Phi_1 + \Phi_2 = 2\pi n, \tag{3}$$

where $k_\perp = \sqrt{2m^* E_{\mathrm{QW}}}/\hbar$ is the momentum wave vector perpendicular to the junction interface, d is the Mg layer thickness, and $\Phi_1 = \Phi_2 = 2\sin^{-1}\sqrt{E_{\mathrm{QW}}/U} - \pi$ is the phase shift on reflection at the Fe/Mg and Mg/MgO interface. Here m^* is the effective mass of Mg electron along the transport direction and can be obtained from the curvature of calculated Mg band dispersion $E(k_z)$ in Fig. 5(e). U is the effective barrier height. By setting the effective barrier height as $U=4.5$ eV for both sets of QWS derived from the two parabolic bands and extracting $m^* \approx 1.1$ and 0.3 from Fig. 5(e), the Mg thickness dependence of the resonance energies in the DOS can

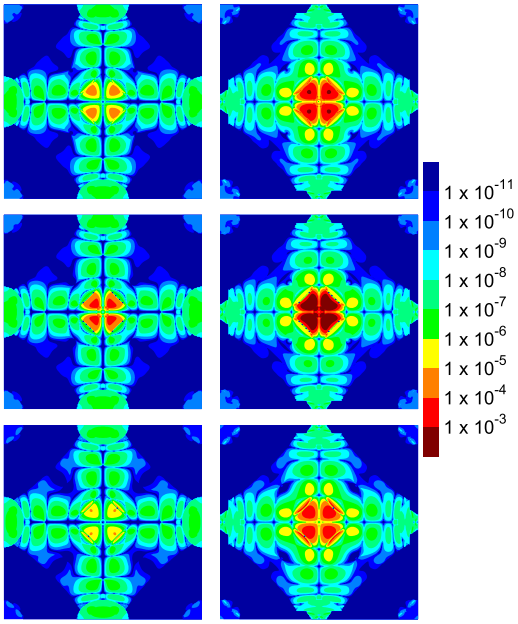

FIG. 6. (Color online) Transmission probability in 2DBZ for -Fe/Mg(2 ML)/MgO/Fe- with three different types of Mg layer spacing at the Fermi energy. The six panels show the transmission for minority-spin in the parallel configuration (left column) and minority-spin to majority-spin in the antiparallel configuration (right column). Type I: first row; type II: second row; and type III: third row. Detailed structures of these three types of junction are discussed in the text.

be fitted perfectly to the QWS given by the PAM. The corresponding numbers of nodes n and n' of these QWS obtained from the PAM are shown in Figs. 5(a)–5(d) for each Mg thickness.

Coupling to the d-IRS in the adjacent Fe layer widens the width of some of the QWS, especially for the QWS at about −0.3 eV for 3 ML Mg thickness. We also note that for Mg thickness larger than 4 ML the $n=0$ QWS falls within the band gap of bulk Mg. This may result from the s-d hybridization on the Fe/Mg interface which can shift the energy levels of Mg QWS. The QWS ranging from −7.5 to −3 eV formed from the lower energy band of bulk Mg are too far away from the Fermi energy thus are not responsible for the resonant tunneling. Because these states are not coupled to the Fe minority-spin d states they provide very good reference points for identifying QWS. In the case of 2 ML Mg, a QWS lays exactly at the Fermi level and couple to a minority-spin d-IRS of adjacent Fe, corresponding to the large resonance peak in minority-spin conductance shown in Fig. 6. There are no QWS at the Fermi energy for other Mg thicknesses. It should also be noted that sharp resonances can be found in Mg within the energy range from −1 to −2.6 eV. They are interfacial resonance state and coupled to the interfacial Fe-layer d states. The positions of these peaks remain almost the same when the thickness of Mg changes.

The QWS in Fig. 5 clearly explain the calculated 2 ML resonant tunneling anomaly shown in Fig. 4. The positions of QWS are highly dependent on the effective Mg layer thickness, which is the width of the quantum well. In actual experiments the effect of QWS may not be easily observed because the junction structures are inevitably susceptible to small perturbations such as strains in the Mg interlayer, and the QWS are very sensitive to even slight change in the Mg thickness. Thus observation of the QWS resonance requires both advanced fabrication technique for high-quality junction interfaces and accurate control of the layer thickness.

To demonstrate how sensitive the quantum-well resonance is to small artificially applied strains in the Mg, three sets of Mg layer spacing are used for transport calculations: 2.570 Å (type I) which is determined from the relaxation calculation mentioned in Sec. II; 2.442 Å (type II) and 2.699 Å (type III) which are decreased and increased 5% of original spacing of 2.570 Å, respectively. Calculated minority-spin $\mathbf{k}_{\parallel}$-resolved transmission probabilities at the Fermi energy are shown in Fig. 6 for junctions with these three sets of Mg layer spacing. The integrated conductances and TMR ratios are shown in Table II. Majority-spin conductances are also shown in Table II but only have a weak dependence on the Mg layer spacing. However, the small changes in the Mg spacing cause large changes in the minority-spin channel. Comparing with the type-I case, in type-II junction $G_{\mathrm{P}}^{\downarrow\downarrow}$ increases by an order of magnitude and $G_{\mathrm{AP}}^{\downarrow\uparrow}$ is about 20 times larger. Increasing the Mg spacing may greatly reduce the minority-spin conductance. The type-III junction shows a much reduced $G_{\mathrm{P}}^{\downarrow\downarrow}$ and $G_{\mathrm{AP}}^{\downarrow\uparrow}$ thus the G_{AP} is very close to G_{P} resulting a smaller negative TMR.

VI. CONCLUSION

In conclusion, our calculation indicates that in -Fe/Mg/MgO/Fe- and -Fe/Mg/MgO/Mg/Fe- MTJs the majority-spin electron wave function with the Δ_1 symmetry decay slower than wave functions with other symmetries in the Mg interlayer, similar to the situation in the MgO barrier. Consequently, the role of a Mg interlayer with a thickness of one or several monolayers is not simply to prevent the interface oxidation or improving the texture of subsequently deposited

TABLE II. Tunneling conductivity (unit: $1/\Omega\mathrm{m}^2$) in various spin channels and conductance ratio of $G_{\mathrm{P}}/G_{\mathrm{AP}}$ for -Fe/Mg(2 ML)/MgO/Fe- with three types of interfaces structures.

Structure	$G_{\mathrm{P}}^{\uparrow\uparrow}$	$G_{\mathrm{P}}^{\downarrow\downarrow}$	$G_{\mathrm{AP}}^{\uparrow\downarrow}$	$G_{\mathrm{AP}}^{\downarrow\uparrow}$	TMR ratio (%)
-Fe/Mg2/MgO/Fe-(type I)	2.01×10^{9}	1.56×10^{8}	4.31×10^{7}	6.10×10^{9}	−184
-Fe/Mg2/MgO/Fe-(type II)	2.33×10^{9}	1.12×10^{9}	4.90×10^{7}	1.01×10^{11}	−2829
-Fe/Mg2/MgO/Fe-(type III)	1.82×10^{9}	6.71×10^{7}	3.76×10^{7}	2.14×10^{9}	−15

MgO(001). A thin Mg interlayer can also act as a spin symmetry filter and produce spin-dependent transport that preferentially filters for the majority-spin Δ_1 states. At certain Mg thickness the TMR is strongly influenced by resonant tunneling, due to minority-spin interfacial resonance states and quantum-well states formed within the Mg interlayer. Our calculation thus provides a theoretical understanding how high TMR ratio can be maintained in MTJs with Mg interlayers.

ACKNOWLEDGMENTS

The authors would like to thank T. Moriyama and J. Q. Xiao for providing their experimental data. The project is supported by the State Key Project of Fundamental Research of Ministry of Science and Technology (Grants No. 2006CB932200 and No. 2010CB934400), National Natural Science Foundation of China (Grants No. 10934099, No. 50928101, and No. 50721001), and Graduate Education Project of Beijing Municipal Commission of Education and K. C. Wong Education Foundation, Hong Kong. A portion of this research is conducted at the Center for Nanophase Materials Sciences, which is sponsored at Oak Ridge National Laboratory by the Division of Scientific User Facilities, Office of Basic Energy Sciences, U.S. Department of Energy (DOE). H.P.C. acknowledges U.S./DOE/BES under Grant No. DE-FG02-02ER45995. The authors acknowledge the UF-HPC center and DOE/NERSC for providing computational resources.

[1] W. H. Butler, X.-G. Zhang, T. C. Schulthess, and J. M. MacLaren, Phys. Rev. B **63**, 054416 (2001).
[2] J. Mathon and A. Umerski, Phys. Rev. B **63**, 220403(R) (2001).
[3] S. S. P. Parkin, C. Kaiser, A. Panchula, P. M. Rice, B. Hughes, M. Samant, and S.-H. Yang, Nature Mater. **3**, 862 (2004).
[4] S. Yuasa, T. Nagahama, A. Fukushima, Y. Suzuki, and K. Ando, Nature Mater. **3**, 868 (2004).
[5] C. Heiliger, P. Zahn, and I. Mertig, Mater. Today **9**, 46 (2006).
[6] D. Waldron, L. Liu, and H. Guo, Nanotechnology **18**, 424026 (2007).
[7] S. Ikeda, J. Hayakawa, Y. M. Lee, F. Matsukura, Y. Ohno, T. Hanyu, and H. Ohno, IEEE Trans. Electron Devices **54**, 991 (2007).
[8] J. P. Velev, P. A. Dowben, E. Y. Tsymbal, S. J. Jenkins, and A. N. Caruso, Surf. Sci. Rep. **63**, 400 (2008).
[9] S. Ikeda, J. Hayakawa, Y. Ashizawa, Y. M. Lee, K. Miura, H. Hasegawa, M. Tsunoda, F. Matsukura, and H. Ohno, Appl. Phys. Lett. **93**, 082508 (2008).
[10] L. Jiang, H. Naganuma, M. Oogane, and Y. Ando, Appl. Phys. Express **2**, 083002 (2009).
[11] K. Tsunekawa, D. D. Djayaprawira, M. Nagai, H. Maehara, S. Yamagata, N. Watanabe, S. Yuasa, Y. Suzuki, and K. Ando, Appl. Phys. Lett. **87**, 072503 (2005).
[12] G. Miao, K. B. Chetry, A. Gupta, W. H. Butler, K. Tsunekawa, D. Djayaprawira, and G. Xiao, J. Appl. Phys. **99**, 08T305 (2006).
[13] T. Moriyama, C. Ni, W. G. Wang, X. Zhang, and J. Q. Xiao, Appl. Phys. Lett. **88**, 222503 (2006).
[14] J. C. Read, P. G. Mather, and R. A. Buhrman, Appl. Phys. Lett. **90**, 132503 (2007).
[15] J. J. Cha, J. C. Read, R. A. Buhrman, and D. A. Muller, Appl. Phys. Lett. **91**, 062516 (2007).
[16] Y. Lu, C. Deranlot, A. Vaurès, F. Petroff, J.-M. Georgea, Y. Zheng, and D. Demailles, Appl. Phys. Lett. **91**, 222504 (2007).
[17] J. C. A. Huang, C. Y. Hsu, W. H. Chen, Y. H. Lee, S. F. Chen, C. P. Liu, and Y. Tzeng, J. Appl. Phys. **104**, 073909 (2008).
[18] L. Ye, C. Lee, J. Syu, Y. Wang, K. Lin, Y. Chang, and T. Wu, IEEE Trans. Magn. **44**, 3601 (2008).
[19] X.-G. Zhang, W. H. Butler, and A. Bandyopadhyay, Phys. Rev. B **68**, 092402 (2003).
[20] C. Tusche, H. L. Meyerheim, N. Jedrecy, G. Renaud, A. Ernst, J. Henk, P. Bruno, and J. Kirschner, Phys. Rev. Lett. **95**, 176101 (2005).
[21] C. Heiliger, P. Zahn, B. Yu. Yavorsky, and I. Mertig, Phys. Rev. B **72**, 180406(R) (2005).
[22] B. Y. Yavorsky and I. Mertig, Phys. Rev. B **74**, 174402 (2006).
[23] D. Waldron, V. Timoshevskii, Y. Hu, K. Xia, and H. Guo, Phys. Rev. Lett. **97**, 226802 (2006).
[24] C. Heiliger, P. Zahn, and I. Mertig, J. Magn. Magn. Mater. **316**, 478 (2007).
[25] C. Heiliger, M. Gradhand, P. Zahn, and I. Mertig, Phys. Rev. Lett. **99**, 066804 (2007).
[26] M. Gradhand, C. Heiliger, P. Zahn, and I. Mertig, Phys. Rev. B **77**, 134403 (2008).
[27] Y. Wang, X. F. Han, and X.-G. Zhang, Appl. Phys. Lett. **93**, 172501 (2008).
[28] P. Bose, P. Zahn, J. Henk, and I. Mertig, *Novel Materials and Devices for Spintronics*, edited by O. G. Heinonen, S. Sanvito, V. A. Dediu, and N. Rizzo, MRS Symposia Proceedings No. 1183 (Materials Research Society, Pittsburgh, 2009).
[29] X. Feng, O. Bengone, M. Alouani, I. Rungger, and S. Sanvito, Phys. Rev. B **79**, 214432 (2009).
[30] G. Autès, J. Mathon, and A. Umerski, Phys. Rev. B **80**, 024415 (2009).
[31] P. Giannozzi, S. Baroni, N. Bonini, M. Calandra, R. Car, C. Cavazzoni, D. Ceresoli, G. L. Chiarotti, M. Cococcioni, I. Dabo, A. Dal Corso, S. Fabris, G. Fratesi, S. de Gironcoli, R. Gebauer, U. Gerstmann, C. Gougoussis, A. Kokalj, M. Lazzeri, L. Martin-Samos, N. Marzari, F. Mauri, R. Mazzarello, S. Paolini, A. Pasquarello, L. Paulatto, C. Sbraccia, S. Scandolo, G. Sclauzero, A. P. Seitsonen, A. Smogunov, P. Umari, and R. M. Wentzcovitch, J. Phys.: Condens. Matter **21**, 395502 (2009).
[32] J. P. Perdew, J. A. Chevary, S. H. Vosko, K. A. Jackson, M. R. Pederson, D. J. Singh, and C. Fiolhais, Phys. Rev. B **46**, 6671 (1992).
[33] H. J. Monkhorst and J. D. Pack, Phys. Rev. B **13**, 5188 (1976).
[34] D. Vanderbilt, Phys. Rev. B **41**, 7892 (1990).
[35] J. M. MacLaren, X.-G. Zhang, W. H. Butler, and X. Wang, Phys. Rev. B **59**, 5470 (1999).
[36] A. Kokalj, Comput. Mater. Sci. **28**, 155 (2003).

[37] Y. Wang, Z.-Y. Lu, X.-G. Zhang, and X. F. Han, Phys. Rev. Lett. **97**, 087210 (2006).
[38] C. Heiliger, P. Zahn, B. Y. Yavorsky, and I. Mertig, Phys. Rev. B **77**, 224407 (2008).
[39] K. D. Belashchenko, J. Velev, and E. Y. Tsymbal, Phys. Rev. B **72**, 140404(R) (2005).
[40] P. M. Echenique and J. B. Pendry, Prog. Surf. Sci. **32**, 111 (1989).
[41] N. V. Smith, N. B. Brookes, Y. Chang, and P. D. Johnson, Phys. Rev. B **49**, 332 (1994).